

pubs.acs.org/cm Article

Photoluminescent $Re_6Q_8I_2$ (Q = S, Se) Semiconducting Cluster Compounds

Craig C. Laing, Jiahong Shen, Daniel G. Chica, Shelby A. Cuthriell, Richard D. Schaller, Chris Wolverton, and Mercouri G. Kanatzidis*



Cite This: Chem. Mater. 2021, 33, 5780-5789



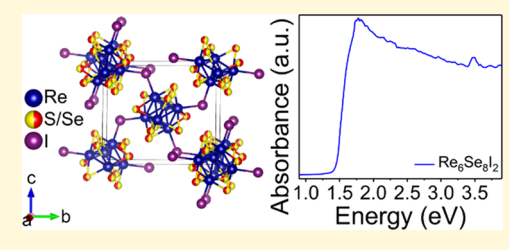
ACCESS

Metrics & More

Article Recommendations

s Supporting Information

ABSTRACT: We report three new rhenium chalcohalide cluster compounds, $Re_6S_8I_2$, $Re_6S_4Se_4I_2$, and $Re_6Se_8I_2$. The materials crystallize in the three-dimensional (3D) $Re_6S_8Cl_2$ structure type with the space group $P2_1/n$. They can be synthesized with sufficiently large iodine gas pressures or using alkali metal iodide salt fluxes with excess iodine. All three compounds are thermally stable under vacuum up to 1000 °C, and density functional theory (DFT) calculation results predict them to be direct-gap semiconductors. The measured work functions, which are the valence band maxima with respect to vacuum, and the measured band gaps are 5.49(5) and 1.69(5) eV, 5.24(5) and 1.54(5) eV, and



5.03(5) and 1.44(5) eV for $Re_6S_8I_2$, $Re_6S_4Se_4I_2$, and $Re_6Se_8I_2$, respectively. They exhibit red to near-IR photoluminescence ranging from 1.38 eV (898 nm) to 1.93 eV (642 nm) centered at 1.67 eV (742 nm) for $Re_6S_8I_2$ and ranging from 1.35 eV (918 nm) to 1.70 eV (726 nm) centered at 1.49 eV (832 nm) for $Re_6Se_8I_2$ with average lifetimes of 5.15 and 1.83 ns, respectively.

■ INTRODUCTION

Rhenium chalcohalides are a family of optically active multianionic hexanuclear rhenium cluster compounds that were initially discovered with the report of Re₆Se₄Cl₁₀ and $Re_6Q_4Br_{10}$ (Q = Se, Te) in 1971. The discovery of KRe₆Se₅Cl₉³ in 1983 was found to be the first soluble rhenium chalcohalide in 1987,4 which was later followed by the discovery of compounds such as Cs5Re6S8Cl7 that contain isolated $[Re_6Q_8X_6]^{4-}$ (Q = S, Se; X = Cl, Br, I) clusters.^{5,6} These soluble sources of [Re₆Q₈X₆]⁴⁻ clusters have enabled a wide variety of solution phase chemistry⁴⁻⁶ including ligandexchange reactions as well as the formation of dimers, dendrimers,^{9,10} supramolecular arrays,^{11,12} and extended frameworks with these clusters.^{13–19} The development of this solution phase chemistry combined with their physical properties that include strong red to near-IR photoluminescence 20-22 and magnetism 23,24 has led to an interest in this family for a variety of potential applications including use in therapeutic agents for cancer treatments, ^{25–29} use as a catalyst, ^{30,31} as well as interest as functionalized two-dimensional (2D) semiconductors that can undergo reversible electrochemical lithium-ion insertion. 32-34 Gabriel et al. further expanded on the chemistry and physical properties of this family of materials.³⁵

The structure and dimensionality of rhenium chalcohalides can be well understood by examining the stepwise dimensional reduction exhibited in the Cs/Re/S/Br system starting with Re₆S₈Br₂, which has three-dimensional (3D) connectivity and is isostructural to Re₆S₈Cl₂. 36,37 The Re₆S₈Br₂ structure derives from [Re₆S₈]²⁺ cluster cores that pack like a body-centered

cubic lattice and covalently link to six neighboring clusters via two different types of bonding schemes. The first bond type is a pair of intercluster Re-S bonds. Each cluster exhibits this type of bonding to two adjacent clusters extending in one crystallographic dimension. The second bond type consists of bridging Re-Br-Re bonds. Each cluster exhibits this type of bonding to four different adjacent clusters, thereby connecting the clusters in three dimensions. The covalent bonds providing this connectivity to six neighboring clusters can be systematically broken through the controlled addition of CsBr equivalents, with the added halide atom terminating the clusters and the Cs atom charge balancing the structure and filling space. The addition of one CsBr equivalent to Re₆S₈Br₂ breaks two of the bridging Re-Br-Re bonds to yield the twodimensional (2D) CsRe₆S₈Br₃. A second equivalent breaks the remaining two bridging halide bonds resulting in onedimensional (1D) cluster chains connected exclusively by Re-S bonds in Cs₂Re₆S₈Br₄.³⁹ With a total of four salt equivalents, the pair of intercluster Re-S bonds are also broken and the cluster is left fully terminated by Br atoms yielding the zerodimensional (0D) Cs₄Re₆S₈Br₆³⁹ structure. It is this 0D structure, which has negatively charged isolated clusters, that enables the solubility of these 0D structures in polar solvents

Received: May 17, 2021 Revised: June 24, 2021 Published: July 12, 2021





such as N_1N -dimethylformamide. $^{5,6,40-42}$ The only structurally distinct iso-stoichiometric chalcohalide to $Re_6S_8Cl_2$ is $Re_6Se_8Cl_2$, which is notable for having a 2D-layered connectivity with the clusters connected exclusively by Re—Se bonds with halide atoms terminating the layers of clusters instead. 36,37,43,44 $Re_6Se_8Cl_2$ does ultimately undergo a similar dimensional reduction with the addition of CsCl equivalents. 5,44

Herein, we describe the structural, thermal, optical, and electronic properties of the rhenium chalcoiodides $Re_6S_8I_2$, $Re_6S_8I_2$, and the solid solution $Re_6S_4S_4I_2$. $Re_6S_8I_2$ and $Re_6S_8I_2$ are the previously undiscovered parent structures for rhenium chalcoiodides. All three crystallize in the monoclinic space group P21/n with the 3D $Re_6S_8Cl_2$ structure type rather than the 2D $Re_6S_8Cl_2$ structure type. A4,45 Synthesis of these materials requires either large iodine pressures or the use of an alkali metal iodide salt flux to overcome the lack of reactivity of gaseous iodine. The compounds are semiconductors and exhibit red to near-IR photoluminescence (PL) with PL lifetimes on the nanosecond time scale, consistent with a direct-gap character.

■ EXPERIMENTAL METHODS

Reagents. NaI (99.8%, Alfa Aesar, Ward Hill, MA), Re (99.997%, ProChem Inc., Alpharetta, GA), S (99.99%, 5N Plus Inc., Saint-Laurent, QC, Canada), Se (99.99%, American Elements, Los Angeles, CA), and $\rm I_2$ (99.8%, Sigma-Aldrich, St. Louis, MO) were used as purchased without additional purification.

 ReQ_2 Synthesis. ReQ_2 (Q = S, Se) was synthesized as a precursor. For both precursors, Re and Q were mechanically mixed in an agate mortar and pestle stoichiometrically in a 1:2 stoichiometry. The amounts used to prepare ReS2 were Re (0.7438 g, 3.995 mmol) and S (0.2562 g, 7.989 mmol). The amounts used to prepare ReSe₂ were Re (0.7438 g, 3.995 mmol) and S (0.2562 g, 7.989 mmol). After mixing the reagents, a fused silica tube with an outer diameter of 10 mm and an inner diameter of 8 mm was charged with the respective mixtures while lined with aluminum foil. This prevents Re powder from sticking to the glass, which can prevent the tube from flame sealing properly. The tube was then evacuated to a pressure of $4.0 \times 10^{-}$ mbar and flame-sealed with a methane and oxygen torch. The tube was then placed in a tube furnace and heated to 425 °C in 5 h, dwelled for 12 h, then ramped to 850 °C in 5 h, dwelled for 24 h, and then the furnace was turned off and allowed to cool to room temperature. Black phase pure polycrystalline powders were obtained for both precursors.

 $Re_6Q_8I_2$ Flux Crystal Growth. Single crystals of $Re_6Q_8I_2$ (Q = S, Se) were synthesized in a NaI flux. $Re_6S_8I_2$ was synthesized using NaI (0.4381 g, 2.923 mmol), Re (0.0726 g, 0.390 mmol), ReS₂ (0.1951 g, 0.7794 mmol), and I₂ (0.2473 g, 0.9742 mmol) in a 15:2:4:5 molar ratio of NaI/Re/ReS₂/I₂. Re₆Se₈I₂ was synthesized using NaI (0.3969 g, 2.648 mmol), Re (0.0657 g, 0.353 mmol), ReSe₂ (0.2430 g, 0.7061 mmol), and I₂ (0.2016 g, 0.7943 mmol) in a 15:2:4:5 molar ratio of NaI/Re/ReSe₂/I₂. The synthesis of Re₆S₄Se₄I₂ as the target stoichiometry was done using NaI (0.3969 g, 2.648 mmol), Re (0.0657 g, 0.353 mmol), ReS₂ (0.2430 g, 0.7061 mmol), ReSe₂ (0.2430 g, 0.7061 mmol), and I₂ (0.2016 g, 0.7943 mmol) in a 15:2:2:2:5 molar ratio of NaI/Re/ReS₂/ReSe₂/I₂. These reagents were loaded in a fused silica tube with a 15 mm outer diameter and a 12 mm inner diameter in air. The tubes were lined with aluminum foil while charging to prevent Re powder from adhering to the glass. The tube was then placed under vacuum until a pressure of 1.0×10^{-2} mbar was reached. The tube was then cooled with liquid nitrogen for 30 s to condense I_2 and then flame-sealed at 4.0×10^{-3} mbar with an inner tube length of 10 cm after sealing. To prevent vapor transport of ReQ2, the sealed tube was positioned in a one-zone tube furnace such that the reagents were adjacent to the thermocouple and the top of the tube was positioned just below the center of the furnace, which is

the hottest region of the tube furnace. Improper placement of the tube resulted in significant transport of ReQ2 out of the salt flux. The furnace was then heated to 850 °C at a rate of 100 °C an hour, held there for 7 days, and then the furnace was turned off and allowed to cool to room temperature. The tube was then opened in a fumehood due to the iodine, and then the product was then placed in methanol. The methanol was then decanted, and the product was washed until the methanol stopped turning purple due to dissolving iodine. The remaining products were needles with surfaces that look dirty with small black powder, which was unreacted Re and ReQ2. To remove the remaining impurities, the product was placed in methanol and sonicated for 5 min and the liquid and anything suspended were decanted. This was repeated for four cycles until the product was single phase by powder X-ray diffraction (PXRD). Re₆S₈I₂ still had a residual ReS2 impurity that was unable to be completely removed. Nitrogen gas was then blown over the remaining crystals to dry them. Crystals that were black needles up to 1 mm long were obtained.

 $Re_6Q_8I_2$ Synthesis under lodine Pressure. $Re_6Q_8I_2$ (Q = S, Se) was synthesized in a pressurized iodine atmosphere. Re₆S₈I₂ was synthesized using Re (0.0726 g, 0.390 mmol) and ReS₂ (0.1951 g, 0.7794 mmol), mechanically mixed in a mortar and pestle in a 1:2 Re/ ReS₂ molar ratio. Re₆Se₈I₂ was synthesized using Re (0.0657 g, 0.353 mmol) and ReSe₂ (0.2430 g, 0.7061 mmol) in a 1:2 Re/ReSe₂ molar ratio. The amount of I2 used was varied for both materials to control the maximum iodine pressure achieved for each reaction. For the 30 atm reactions, 0.1473 g (0.5804 mmol I₂) was used. For the 45 atm reactions, 0.2208 g (0.8700 mmol I_2) was used. For the 60 atm reactions, 0.2941 g (1.159 mmol I2) was used. For the 75 atm reactions, 0.3700 g (1.458 mmol I₂) was used. The tubes were lined with aluminum foil while charging to prevent Re powder from adhering to the glass. Fused silica tubes with an outer diameter of 10 mm and an inner diameter of 6 mm were used and then sealed with an inner length of 10 cm and an outer length of 11.5 cm for a consistent volume for each reaction. The tube was then placed under vacuum until a pressure of 1.0×10^{-2} mbar was reached. The tube was then cooled with liquid nitrogen for 30 s to condense I2 and then flame-sealed at 4.0×10^{-3} mbar. For the 45, 60, and 75 atm reactions, the sealed tube was then placed in a second fused silica tube along with 0.2060 g (0.8116 mol) of I₂ for the 45 and 60 atm reactions or 0.3169 g (1.249 mmol) of I₂. The second tube had an outer diameter of 15 mm, an inner diameter of 12 mm, and an internal length of 16 cm and flame-sealed with an identical liquid nitrogen process to condense the iodine for an estimated maximum pressure of either 14 or 23 atm in the second outer tube. To prevent vapor transport of ReQ2, the reaction tube was positioned in a one-zone tube furnace such that the reagents were adjacent to the thermocouple and the top of the reaction tube was positioned just below the center of the furnace, which is the hottest region of the furnace. The furnace was then heated to 850 °C at a rate of 100 °C an hour, held there for 4 days, and then the furnace was turned off and allowed to cool to room temperature. To calculate an estimated maximum pressure of iodine in each reaction vessel, a few assumptions were made in an effort to ensure that the tubes did not explode upon heating a gas in a closed container and to estimate how this parameter was varied. These assumptions were that the iodine was the gas in the container, that the pressure could be estimated by the ideal gas law, that the internal volume could be approximated by a cylinder, that at 850 °C, 60% of I₂ molecules dissociate into two iodine molecules based on the work of DeVries and Rodebush, 46 and that the volume occupied by the Re and ReQ2 was negligible and could be ignored. To increase the range of accessible pressures, the second tube was pressurized using I2 to achieve a larger external pressure. The pressure in the outer tube was then estimated with the same assumptions along with a volume subtraction for the reaction vessel based on the outer diameter instead of the inner diameter.

Single-Crystal X-ray Diffraction. Intensity data of black needle-shaped single crystals grown from the flux method of $Re_6S_8I_2$, $Re_6S_4Se_4I_2$, and $Re_6Se_8I_2$ were collected at 293 K. Suitable single crystals with dimensions of $0.009 \times 0.008 \times 0.023$ mm³, $0.006 \times 0.006 \times 0.011$ mm³, and $0.011 \times 0.012 \times 0.035$ mm³, respectively,

Table 1. Crystal Data and Structure Refinement at 293(2) Ka

empirical formula	$\mathrm{Re}_6\mathrm{S}_8\mathrm{I}_2$	$Re_6S_4Se_4I_2$	$Re_6Se_8I_2$
formula weight	1627.48	1815.08	2002.68
temperature (K)	293(2)	293(2)	293(2)
wavelength (Å)	0.56083	0.56083	0.56083
crystal system	monoclinic	monoclinic	monoclinic
space group	P21/n	P21/n	P21/n
unit cell dimensions	a = 6.3649(13) Å	a = 6.4555(13) Å	a = 6.5735(13) Å
	b = 11.607(2) Å	b = 11.848(2) Å	b = 12.029(2) Å
	c = 10.177(2) Å	c = 10.308(2) Å	c = 10.402(2) Å
	$\alpha = 90^{\circ}$	$\alpha = 90^{\circ}$	$\alpha = 90^{\circ}$
	$\beta = 98.77(3)^{\circ}$	$\beta = 99.20(3)^{\circ}$	$\beta = 99.63(3)^{\circ}$
	$\gamma = 90^{\circ}$	$\gamma = 90^{\circ}$	$\gamma = 90^{\circ}$
volume (ų)	743.0(3)	778.3(3)	810.9(3)
Z	2	2	2
density (calculated) (g/cm³)	7.274	7.746	8.202
absorption coefficient (mm ⁻¹)	28.940	32.310	35.501
F(000)	1368	1512	1656
crystal size (mm³)	$0.023 \times 0.009 \times 0.008$	$0.011 \times 0.006 \times 0.006$	$0.035 \times 0.012 \times 0.011$
heta range for data collection (deg)	2.114-27.998	2.713-26.495	2.672-26.499
index ranges	$-10 \le h \le 10$	$-9 \le h \le 10$	$-9 \le h \le 10$
	$-19 \le k \le 18$	$-18 \le k \le 18$	$-19 \le k \le 18$
	$-17 \le l \le 16$	$-16 \le l \le 16$	$-16 \le l \le 16$
reflections collected	10 313	8995	9869
independent reflections	$3639 [R_{\rm int} = 0.0346]$	$3264 [R_{int} = 0.0477]$	$3400 [R_{\rm int} = 0.0437]$
completeness to θ = 19.664 $^{\circ}$	99.4%	99.6%	98.7%
refinement method	full-matrix least-squares on F^2	full-matrix least-squares on F^2	full-matrix least-squares on F^2
data/restraints/parameters	3639/0/73	3264/1/77	3400/0/73
goodness-of-fit	1.091	1.031	1.101
final R indices $[I > 2\sigma(I)]$	$R_{\rm obs} = 0.0420, \ wR_{\rm obs} = 0.0977$	$R_{\rm obs} = 0.0478$, $wR_{\rm obs} = 0.1034$	$R_{\rm obs} = 0.0458$, $wR_{\rm obs} = 0.0961$
R indices [all data]	$R_{\rm all} = 0.0563$, $wR_{\rm all} = 0.1033$	$R_{\rm all} = 0.0789$, w $R_{\rm all} = 0.1149$	$R_{\rm all} = 0.0802$, w $R_{\rm all} = 0.1043$
largest diff. peak and hole	3.191 and $-3.672 \text{ e}\cdot\text{Å}^{-3}$	$3.393 \text{ and } -2.918 \text{ e} \cdot \text{Å}^{-3}$	$4.285 \text{ and } -4.033 \text{ e} \cdot \text{Å}^{-3}$
$R = \sum F_0 - F_c / \sum F_0 , wR = \sum [u]$	$v(F_{\rm o} ^2 - F_{\rm c} ^2)^2] / \sum [w(F_{\rm o} ^4)]^{1/2}$ and	$w = 1/[\sigma^2(F_o^2) + (0.1135P)^2]$, whe	re $P = (F_o^2 + 2F_c^2)/3$.

were mounted on a glass fiber with superglue on a STOE StadiVari diffractometer equipped with an AXO Auxilia Microfocus Ag K α (λ = 0.56083 Å)-sealed X-ray source and a Dectris Pilatus3 R CdTe 300K Hybrid Photon Counting detector. Data reduction was performed with the STOE X-Area version 1.90 software package using a numerical absorption correction using STOE X-Red version 1.65.2 and STOE X-Shape version 2.21 followed by scaling and outlier rejection with the STOE LANA version 1.83.8. 47 The structure was solved with the ShelXT 48 structure solution program using the intrinsic phasing solution method and using Olex2 49 as the graphical interface. The model was refined with ShelXL 50 using least-squares minimization. The crystallographic information can be found in Tables 1–4 and S1–S9.

Photoluminescence and Time-Resolved Photoluminescence (trPL). Spectroscopic measurements were performed using a Ti:sapphire amplifier with a 2 kHz repetition rate and a 35 fs pulse width. Samples were excited using 400 nm pump pulses generated via a frequency-doubled 800 nm output produced using a BBO crystal. A single-photon-sensitive streak camera with a 0.15 m spectrograph was used to measure time-resolved photoluminescence.

Density Functional Theory (DFT) Calculations. All density functional theory (DFT)^{\$1,52} calculations were carried out using the Vienna ab initio simulation package (VASP)^{\$3,54} with the projector-augmented wave (PAW)^{\$55} method. The Perdew–Burke–Ernzerhof (PBE)^{\$66} generalized gradient approximation (GGA) was chosen as the exchange–correlation functional. The plane-wave cutoff energy was set to \$20 eV, and the structures were fully relaxed until the total energy converges to 10^{-8} eV and the force on each atom is less than 0.001 eV/Å. Γ-Centered k-point meshes were constructed with at least 8000 k-points per reciprocal atom (KPPRA). Phonon calculations were performed with the 2 × 2 × 2 supercell using the

Table 2. Atomic Coordinates $(\times 10^4)$ and Equivalent Isotropic Displacement Parameters $(\mathring{A}^2\times 10^3)$ for $Re_6S_8I_2$ at 293(2) K with Estimated Standard Deviations in Parentheses

label	\boldsymbol{x}	у	z	occupancy	$U_{\rm eq}^{a}$
Re(1)	2485(1)	5269(1)	5607(1)	1	15(1)
Re(2)	5872(1)	6486(1)	5452(1)	1	15(1)
Re(3)	6177(1)	4476(1)	6657(1)	1	15(1)
S(1)	9183(4)	5701(2)	6525(3)	1	18(1)
S(2)	2398(4)	7085(2)	4481(3)	1	19(1)
S(3)	4543(4)	6121(2)	7503(3)	1	18(1)
S(4)	2957(4)	3433(2)	6687(3)	1	18(1)
I(1)	7863(2)	3773(1)	9194(1)	1	24(1)

 $^aU_{\rm eq}$ is defined as one-third of the trace of the orthogonalized $U_{\rm ij}$ tensor.

PHONOPY package. The thermodynamic stabilities of $Re_6Q_8I_2$ compounds were evaluated using the convex hull method implemented in the Open Quantum Materials Database (OQMD). 59,60

RESULTS AND DISCUSSION

Crystal Structure. All three $Re_6Q_8I_2$ (Q = S, Se) compounds are isostructural and crystallize in the 3D $Re_6S_8Cl_2$ structure type³⁷ with the space group P21/n shown in Figure 1. Each cluster contains six rhenium atoms in the +3 oxidation state whose coordination to each other forms an octahedron where each Re atom occupies a corner. The eight

Table 3. Atomic Coordinates $(\times 10^4)$ and Equivalent Isotropic Displacement Parameters $(\mathring{A}^2 \times 10^3)$ for $Re_6S_4Se_4I_2$ at 293(2) K with Estimated Standard Deviations in Parentheses

label	\boldsymbol{x}	у	z	occupancy	$U_{\rm eq}^{a}$
Re(1)	2514(1)	5245(1)	5610(1)	1	18(1)
Re(2)	5872(1)	6456(1)	5491(1)	1	18(1)
Re(3)	6194(1)	4448(1)	6629(1)	1	18(1)
S(1)	9252(3)	5702(2)	6611(2)	0.536(3)	28(1)
Se(1)	9252(3)	5702(2)	6611(2)	0.464(3)	28(1)
S(2)	2335(3)	7129(2)	4541(2)	0.509(3)	23(1)
Se(2)	2335(3)	7129(2)	4541(2)	0.491(3)	23(1)
S(3)	4586(3)	6070(2)	7601(2)	0.518(3)	23(1)
Se(3)	4586(3)	6070(2)	7601(2)	0.482(3)	23(1)
S(4)	2950(3)	3369(2)	6697(2)	0.437(3)	25(1)
Se(4)	2950(3)	3369(2)	6697(2)	0.563(3)	25(1)
I(1)	7929(2)	3712(1)	9118(1)	1	29(1)

 $[^]aU_{
m eq}$ is defined as one-third of the trace of the orthogonalized $U_{
m ij}$ tensor.

Table 4. Atomic Coordinates $(\times 10^4)$ and Equivalent Isotropic Displacement Parameters $(\mathring{A}^2 \times 10^3)$ for $Re_6Se_8I_2$ at 293(2) K with Estimated Standard Deviations in Parentheses

label	\boldsymbol{x}	у	z	occupancy	$U_{\rm eq}^{a}$
Re(1)	2551(1)	5226(1)	5608(1)	1	7(1)
Re(2)	5866(1)	6435(1)	5518(1)	1	7(1)
Re(3)	6201(1)	4427(1)	6614(1)	1	7(1)
Se(1)	9286(2)	5675(2)	6628(2)	1	9(1)
Se(2)	2333(2)	7120(2)	4580(2)	1	11(1)
Se(3)	4616(2)	6028(2)	7637(2)	1	10(1)
Se(4)	2969(2)	3343(2)	6660(2)	1	10(1)
I(1)	7038(2)	8664(1)	5930(1)	1	17(1)

 $^{a}U_{\mathrm{eq}}$ is defined as one-third of the trace of the orthogonalized U_{ij} tensor.

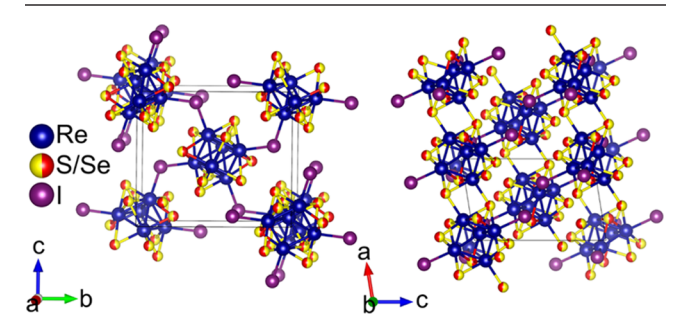


Figure 1. Crystal structure of $\text{Re}_6\text{Q}_8\text{I}_2$ looking down the *a*-axis on the left and down the *b*-axis on the right.

faces of the octahedra are capped by a chalcogenide atom forming a $[Re_6Q_8]^{2+}$ cluster core. The cluster cores pack in a body-centered cubic-type arrangement but are only covalently bonded to six of the eight nearest clusters. The two types of bridging interactions are Re–I–Re bonding that four rhenium atoms per cluster participate in and Re–Q bonding that the other two rhenium atoms participate in. The Re–Re bond lengths in the cluster core are similar in length, with the shortest bond lengths of 2.5880(9), 2.6014(10), and 2.6118(9) Å in $Re_6S_8I_2$, $Re_6S_4Se_4I_2$, and $Re_6Se_8I_2$, respectively. These Re–Re bond lengths are all shorter than the 2.7476(17) Å bond observed in rhenium metal, 61 longer than the 2.46 Å found in

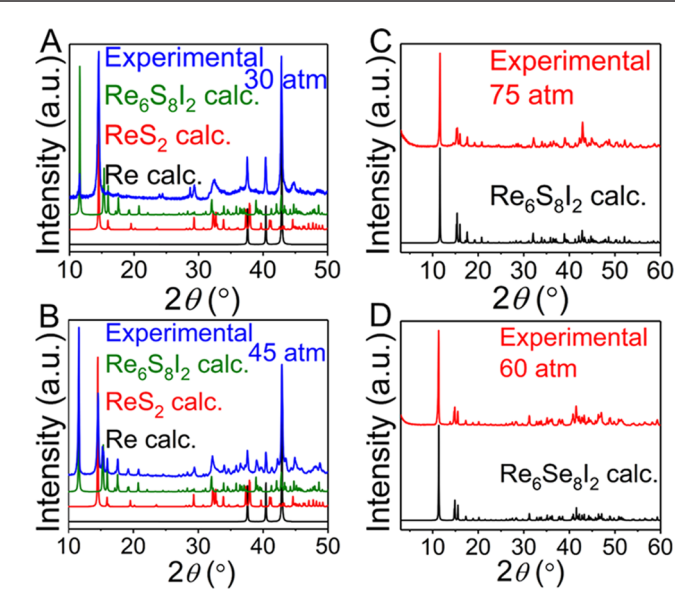


Figure 2. PXRD patterns showing reaction progression as a function of the estimated maximum iodine pressure for $Re_6S_8I_2$ at (A) \sim 30 atm, (B) \sim 45 atm, (C) \sim 75 atm, and (D) $Re_6Se_8I_2$ at \sim 60 atm. At \sim 75 atm for $Re_6S_8I_2$ and \sim 60 atm for $Re_6Se_8I_2$, the reaction is nearly complete with a residual ReQ_2 peak at around 14° 2θ .

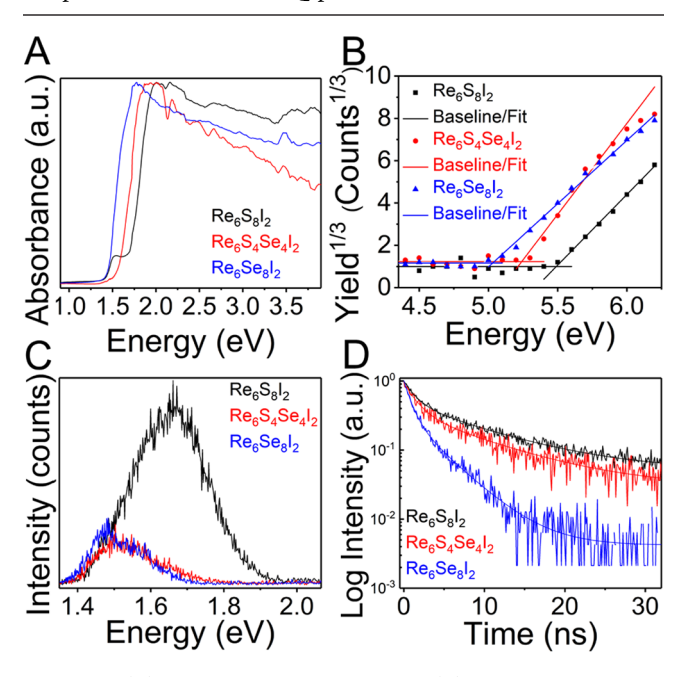


Figure 3. (A) Optical absorption spectra, (B) photoemission yield spectroscopy in air where the baseline and fit intercept signify the energy position of the valence band maxima, (C) photoluminescence spectra produced using a 400 nm excitation at room temperature, and (D) time-resolved photoluminescence dynamics measured at the emission maxima shown in (C) at room temperature.

 Re_3I_9 , ⁶² which has trinuclear 3+ rhenium clusters, and slightly longer than the 2.5803(8) Å observed in $Re_6S_8Cl_2$. ³⁷

Each face of the rhenium octahedra is capped by a chalcogenide atom that bonds to three of the rhenium atoms, which is a μ_3 -type interaction. For six of the eight chalcogenide atoms, this face capping μ_3 -type interaction is the only bonding interaction they participate in. The Re–Q bond lengths for this interaction are similar, with the shortest bond lengths of 2.375(3), 2.464(2), and 2.4998(16) Å in Re₆S₈I₂,

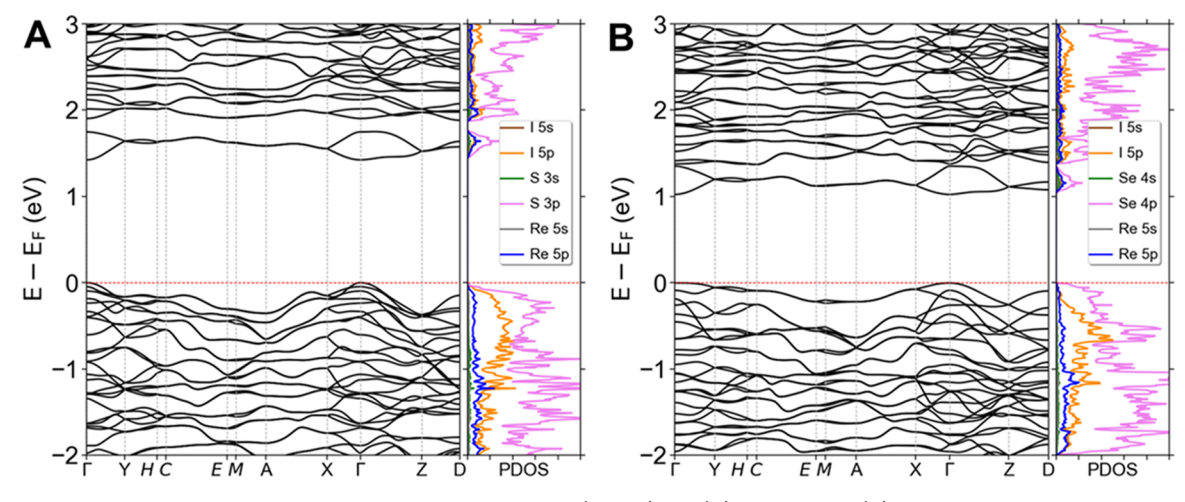


Figure 4. Calculated electronic structure and partial density of states (PDOS) for (A) Re₆S₈I₂ and (B) Re₆Se₈I₂.

Re₆S₄Se₄I₂, and Re₆Se₈I₂, respectively. These bond lengths are reasonable when compared with the shortest Re-Q lengths seen in ReQ₂, 2.331(7) Å for Re-S⁶³ and 2.3818(3) Å for Re-Se⁶³ and those seen in Re₆S₈Cl₂ with a Re-S bond length of 2.374(3) Å.³⁷ The remaining two chalcogenide atoms are on opposite sides of the cluster, and each participates in an intercluster Re-Q bridging bond in addition to the three Re-Q bonds that cap one face of the rhenium octahedra adopting a μ_4 type. Of these four Re-Q bonds, two of the bonds are about 0.1 Å shorter than the other two with bond lengths. In Re₆S₈I₂, the two shorter bond lengths are 2.400(3) and 2.404(3) Å compared to 2.478(3) and 2.530(3) Å for the two longer bonds. The two shorter bonds are to two rhenium atoms, which participate in Re-I-Re bridging μ_2 -type interactions. The longest bond is to the third rhenium atom on the same cluster, which has a bridging Re-S bond, while the bridging Re-S bond to the rhenium on the adjacent cluster has the second-longest bond length of 2.478(3) Å. This trend is observed in both $Re_6S_4Se_4I_2$ and $Re_6Se_8I_2$ as well as in Re₆S₈Cl₂, in which the sulfur with four Re-S bonds has two 2.398(4) Å bonds, a longer 2.536(3) Å bond, and a 2.480(4) Å bridging bond.³⁷

The four rhenium atoms that do not participate in bridging Re–Q bonds instead each have bridging Re–I–Re μ_2 -type interactions. The Re–I bond lengths on either side of a given iodine atom are nearly identical, with the shortest lengths of 2.7639(11), 2.7717(13), and 2.7784(13) Å for Re₆S₈I₂, Re₆S₄Se₄I₂, and Re₆Se₈I₂, respectively. This is very similar to the Re–I bond length in ReI₃ for the μ_2 iodine atoms of 2.743 (5) Å as opposed to the longer terminal Re–I bond length of 2.947 Å in ReI₃. This is also longer than the Re–Cl–Re bonds observed in Re₆S₈Cl₂ of 2.444(4) and 2.468(4) Å. These bridging interactions connect the cluster cores in the $(\overline{1}01)$ plane, which when combined with the bridging Re–Q interactions results in the 3D connectivity of the clusters.

The chemical composition for all three materials was corroborated using energy-dispersive spectroscopy (EDS) in a scanning electron microscope (SEM) shown in the Supporting Information. For the 1:1 sulfur-to-selenium solid solution, the ratio of the chalcogenides was examined with both EDS and through the crystallographic refinement. Both found the crystal to be slightly sulfur-rich, with the EDS giving elemental ratios of $Re_{6.00}S_{4.55}Se_{3.99}I_{2.13}$ while freely refining all of the chalcogenide sites as fully occupied mixed sites gave a

composition of Re₆S_{4.13}Se_{3.87}I₂. Since the deviation from 1:1 is not statistically significant for qualitative EDS, the structure refinement value was nearly 1:1, and the material was prepared from precursors with a 1:1 sulfur-to-selenium stoichiometry, the total occupancy of the chalcogenides was then fixed to a 1:1 ratio for the final structure refinement. There are four different chalcogenide sites in the asymmetric unit of the structure, and the occupancy of the two chalcogenides in each of the four sites was allowed to freely refine. One of the four sites corresponds to the chalcogenide that bridges cluster units. This site was found to have a mild preference for sulfur with a 53.6(3)% sulfur occupation to 46.4(3)% selenium occupation. The three other sites are the nonbridging chalcogenide atoms with occupancies of 50.9(3)% S/49.1(3)% Se, 51.8(3)% S/48.2(3)% Se, and 43.7(3)% S/56.3(3)% Se.

Synthesis and Thermal Characterization. The synthesis of pure Re₆Q₈I₂ can be challenging and requires careful consideration due to the limited reactivity of gaseous iodine. A stoichiometric combination reaction of either the elements or of Re, ReQ2, and I2 at 850 °C is unable to form the target compounds. Two different approaches were used to overcome this challenge: large iodine pressures and alkali metal iodide fluxes. The use of large iodine pressures requires careful control of the reaction conditions to prevent the fused silica tube from exploding due to internal pressure. To prevent the sealed tube from breaking (observed for the estimated pressures of 60 and 75 atm), it was placed inside a second larger silica tube along with additional iodine to reduce the pressure differential inside the reaction vessel and outside the reaction depicted in the Supporting Information. A full description of the reaction parameters and the method used to estimate the pressure inside the reaction vessel can be found in the Experimental Methods section. How far the reaction could proceed for identical heating profiles was determined as a function of the estimated maximum pressure by PXRD of the material. As shown in the X-ray diffraction pattern in Figure 2, the Re₆Q₈I₂ peak at 11.61° 2θ can be observed for the 30 atm reaction as a minority phase and becomes the dominant peak in the pattern in the 45 atm reaction, while the relative intensity of the ReS2 Bragg peak at 14.59° (or the ReSe2 at 13.86°) $2\theta^{63}$ has substantially dropped. For the 75 atm Re₆S₈I₂ reaction and the 60 atm Re₆Se₈I₂ shown in Figure 2C,D, the reaction has nearly reached completion, with the ReQ2 peak having almost completely disappeared. We conclude that the

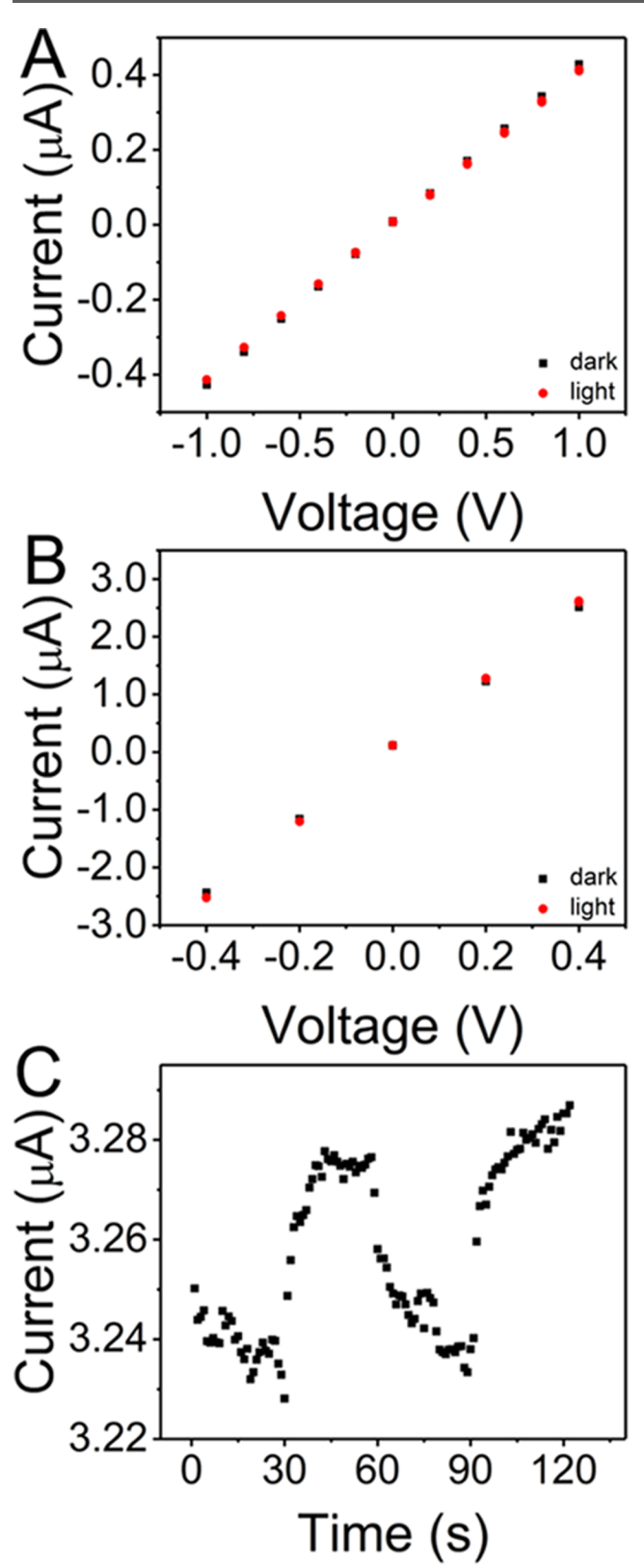


Figure 5. Electrical resistivity measurements of (A) $Re_6S_8I_2$, (B) $Re_6Se_8I_2$, and (C) on/off light response of $Re_6Se_8I_2$ for two cycles of 30 s intervals of dark and then light response.

selenide reaction requires less iodine pressure to progress than the sulfide as evidenced by this difference in the required pressure to reach near completion. The excess iodine can be removed from the product in a variety of ways including methanol washes, using a gentle flame while the tube is still sealed to transport the iodine to the other end of the tube, gently heating the product on a hot plate or even allowing the product to sit in a fumehood for several hours and returning to the product later. It is strongly recommended that the tube is opened in a fumehood upon completion to prevent irritation from the iodine.

The synthesis of Re₆Q₈I₂ crystals up to 1 mm long was achieved via sodium iodide fluxes. It is important to note when using this method that the selection of an alkali metal that is too large will result in a dimensionally reduced cluster. Sodium was found to be sufficiently small to provide a nonreactive flux medium for the synthesis of these phases for both the sulfide and the selenide, with no trace of Na in the EDS. Crystal growth was achieved using NaI and excess I2 with Re and ReQ2 in a 1:2 ratio. The estimated maximum iodine pressure used was 10 atm, which is below the pressure where the formation of Re₆Q₈I₂ was observed without the flux. It is likely that the molten salt enables some of the iodine to dissolve into solution (possible via the equilibrium reaction $I_2 + I^- \rightarrow I_3^-$), which would imply that the real pressure in the tube is actually lower than the estimated pressure and instead enables the iodine to react with Re and ReS2 from a more reactive liquid state without the larger iodine pressure needed to otherwise drive the reaction. The crystals grown from this flux method were largest for the sulfide and smallest for the selenide, with the solid solution crystals generally in between. ReQ2 grows as black platelets, which look like black needles when they are sufficiently small and are nearly indistinguishable by eye preventing mechanical separation. The crystal size distribution shown in Figure S2 was representative after the washing procedure. Most crystals of $Re_6S_8I_2$ were 100-500 μm in length, $Re_6S_4Se_4I_2$ were 50-200 μm in length, and $Re_6Se_8I_2$ were around 50–100 μm in length. Select crystals for Re₆Se₈I₂ and Re₆S₄Se₄I₂ were found to reach lengths up to 1 mm, but far fewer were observed for Re₆Se₈I₂ than for the solid solution. In the case of Re₆S₈I₂ crystals, up to 2 mm in length were obtained using this flux method. The crystals grown by this method were also found to frequently grow as twinned crystals. This was often difficult to tell by eye but easily observed when performing indexation when testing crystals for single-crystal diffraction for crystals 100 μ m or longer.

Differential thermal analysis (DTA) was used to determine the thermal stability and is shown in Figure S5. All compounds had no thermal events up to 1000 °C under vacuum, and the PXRD shown in the Supporting Information before and after DTA was unchanged indicating thermal stability under vacuum up to 1000 °C. The theoretical thermodynamic stabilities of both Re₆S₈I₂ and Re₆Se₈I₂ were also evaluated through the Open Quantum Materials Database (OQMD) and both of them are calculated as stable. They are 97 and 111 meV/atom deep in the convex hull, respectively, showing additional evidence of being thermodynamically stable.

Optical and Electronic Properties. To study the optical properties and to determine the energy levels of the valence band maximum (VBM) and conduction band minimum (CBM), UV—vis diffuse reflectance spectroscopy and photoemission yield spectroscopy in air ^{64,65} (PYSA) measurements were performed on samples synthesized via the flux synthesis method. The diffuse reflectance data was transformed with the Kubelka—Munk equation ⁶⁶ into absorbance data shown in Figure 3A, where the absorption edge was determined by extrapolating the linear region. For Re₆S₈I₂, a small feature

below the absorption edge was fit to the absorption spectra of the ${\rm ReS}_2$ impurity, which is shown in Figure S10 and also observed in the PXRD.

The band gaps of the three phases were found to be 1.69(5) eV (734 nm) for $Re_6S_8I_2$, 1.54(5) eV (805 nm) for $Re_6S_4Se_4I_2$, and 1.44(5) eV (861 nm) for $Re_6Se_8I_2$. A linear extrapolation of the PYSA data shown in Figure 3B was used to determine the work function, which is also the VBM. This was found to be 5.49(5) eV (226 nm) for $Re_6S_8I_2$ and 5.24(5) eV (237 nm) and 5.03(5) eV (246 nm) for $Re_6Se_8I_2$ with respect to vacuum. Using these values in combination with the absorption edges yields CBM values of 3.80(7) eV (326 nm) for $Re_6S_8I_2$, 3.70(7) eV (335 nm) for $Re_6S_4Se_4I_2$, and 3.59(7) eV (345 nm) for $Re_6Se_8I_2$ with respect to vacuum.

The room-temperature photoluminescence (PL) and the time-resolved photoluminescence (trPL) for all three materials are shown in Figure 3C,3D, respectively. Red to near-IR emission was observed for all three materials with a range of 1.38 eV (898 nm)-1.93 eV (642 nm) centered at 1.67 eV (742 nm) for Re₆S₈I₂ and 1.35 eV (918 nm)-1.70 eV (729 nm) centered at 1.49 eV (832 nm) for Re₆Se₈I₂. The solid solution Re₆S₄Se₄I₂ exhibited emission more similar to Re₆Se₈I₂ than to Re₆S₈I₂ ranging from 1.38 eV (898 nm) to 1.75 eV (708 nm) centered at 1.52 eV (816 nm). The trPL for all three materials were fit to a biexponential function (see the Supporting Information). The average lifetime was longest for $Re_6S_8I_2$ at 5.15 \pm 0.23 ns and decreased across the series with 4.34 ± 0.39 ns for Re₆S₄Se₄I₂ and 1.83 ± 0.09 ns for Re₆Se₈I₂. The observed photoluminescence features are comparable to the tetra-n-butylammonium (n-Bu₄N) salt derivative, (n-Bu₄N)₄Re₆S₈I₆, ²⁰⁻²² which contains the isolated [Re₆Q₈X₆]⁴⁻ cluster unit and has demonstrated similar PL properties. For such 0D iodide-containing clusters, the PL maximum is at 1.55 eV (800 nm). Additionally, we see that the dimensional reduction of the clusters increases the room-temperature PL lifetimes.

The calculated band structure and partial density of states (PDOS) for Re₆S₈I₂ and Re₆Se₈I₂, shown in Figure 4, predict that both materials are direct-gap semiconductors where the VBM and CBM occur at the Γ point. The calculated band gaps are 1.42 and 1.03 eV for Re₆S₈I₂ and Re₆Se₈I₂, respectively. These values are slightly smaller than the measured values, which is reasonable since DFT is known to underestimate the band gaps of semiconductors.⁶⁷ For Re₆Se₈I₂, the conduction band is more dispersive than the valence band at the Γ point. The carrier effective masses at the Γ point calculated in the direction of X for the electrons are 1.956 m_0 compared to an effective mass of the holes of $-2.576 m_0$. The bands for Re₆S₈I₂ are more dispersive than those for Re₆Se₈I₂, and the valence band is more dispersive than the conduction band. Both carriers are also lighter in Re₆S₈I₂, with an effective mass of 1.574 m_0 and -0.556 m_0 for the electron and the hole in the same direction of Γ to X. The difference occurs as a result of how much the chalcogenide contributes to the top of the valence band, as seen in the PDOS. In the selenide, there are Se 4p orbital contributions to the top of the VBM that are slightly higher in energy than the I 5p orbital contribution, while in the sulfide, the S 3p contributions start contributing significantly at about the same energy as the I 5p orbitals. This is attributed to the lower electronegativity of selenium compared to those of iodide and sulfide atoms. The orbital state contributions to the CBM meanwhile are similar in both materials, coming primarily from either S 3s and 3p or Se 4s

and 4p, Re 5p, and I 5p orbitals. The calculated phonon structure and PDOS show slightly lower-energy vibrations for $Re_6Se_8I_2$ than for $Re_6S_8I_2$, with the lowest-energy modes primarily having contributions from Re and I with a bit more of a contribution from Se than from S around 50 cm⁻¹ (Figure S9).

The electrical photoconductivity response in ambient light is shown in Figure 5, measured using crystals grown from the flux method for $Re_6S_8I_2$ (0.0016 cm² cross section, 0.20 cm length) and $Re_6S_8I_2$ (0.00010 cm² cross section, 0.10 cm length). Both materials exhibited ohmic behavior with no hysteresis for two cycles in both the light and the dark. For $Re_6S_8I_2$, the dark resistance was $2.37\times 10^6~\Omega$ with a dark resistivity of $1.9\times 10^4~\Omega$ ·cm, while the light resistance was $2.44\times 10^6~\Omega$ with a light resistivity of $2.0\times 10^4~\Omega$ ·cm. For $Re_6Se_8I_2$, the dark resistance was $1.63\times 10^5~\Omega$ with a dark resistivity of $1.6\times 10^2~\Omega$ ·cm, while the light resistance was $1.58\times 10^5~\Omega$ with a light resistivity of $1.6\times 10^2~\Omega$ ·cm. The light response was also measured for $Re_6Se_8I_2$ for two cycles of 30 s in the dark and then in the light with a 1.2% current change of 40 nA.

CONCLUSIONS

The new members of the rhenium chalcohalide family, $Re_6S_8I_2$, $Re_6S_4Se_4I_2$, and $Re_6Se_8I_2$, adopt the $R_6S_8Cl_2$ 3D structure type. Sufficiently large iodine pressures must be used to increase the reactivity of the iodine and drive the formation of the cluster or the use of an alkali metal iodide salt flux can be used to grow crystals. $Re_6S_8I_2$ and $Re_6Se_8I_2$ are both direct-gap semiconductors at the Γ point with band gaps of 1.69(5) and 1.44(5) eV. The energies of the valence band maxima for $Re_6S_8I_2$, $Re_6S_4Se_4I_2$, and $Re_6Se_8I_2$ were measured at 5.49(5), 5.24(5), and 5.03(5) eV, respectively. The compounds exhibit broad red to near-IR photoluminescence (PL) centered at 1.67 eV (742 nm) for $Re_6S_8I_2$, 1.52 eV (816 nm) for $Re_6S_4Se_4I_2$, and 1.49 eV (832 nm) for $Re_6Se_8I_2$. The PL average lifetimes were found to be 5.15 ± 0.23 , 4.34 ± 0.39 , and 1.83 ± 0.09 ns for $Re_6S_8I_2$, $Re_6S_4Se_4I_2$, and $Re_6Se_8I_2$, respectively.

■ ASSOCIATED CONTENT

Supporting Information

The Supporting Information is available free of charge at https://pubs.acs.org/doi/10.1021/acs.chemmater.1c01696.

Table S1: Re₆S₈I₂ crystallographic anisotropic data; Table S2: Re₆S₈I₂ crystallographic bond lengths; Table S3: Re₆S₈I₂ crystallographic bond angles; Table S4: Re₆S₄Se₄I₂ crystallographic anisotropic data; Table S5: Re₆S₄Se₄I₂ crystallographic bond lengths; Table S6: Re₆S₄Se₄I₂ crystallographic bond angles; Table S7: Re₆Se₈I₂ crystallographic anisotropic data; Table S8: Re₆Se₈I₂ crystallographic bond lengths; Table S9: Re₆Se₈I₂ crystallographic bond angles; Table S10: Pl lifetime fit values; Figure S1: diagram of high-pressure reaction setup; Figure S2: picture of crystals grown from flux reactions; Figure S3: SEM images of crystals grown from flux reactions; Figure S4: EDS of crystals grown from flux reactions; Figure S5: differential thermal analysis; Figure S6: PXRD of Re₆S₈I₂ before and after DTA; Figure S7: PXRD of Re₆S₄Se₄I₂ before and after DTA; Figure S8: PXRD of Re₆Se₈I₂ before and after DTA; Figure S9: phonon structure and partial density of states; Figure S10: diffuse reflectance comparison of impurity feature with ReS2; and Figure S11: phase

percentage determination from PXRD for ReS_2 impurity in $Re_6S_8I_2$ (PDF)

CSD deposit number for Re₆S₈I₂: 2083085 (CIF)

CSD deposit number for Re₆S₄Se₄I₂: 2083084 (CIF)

CSD deposit number for Re₆Se₈I₂: 2083086 (CIF)

AUTHOR INFORMATION

Corresponding Author

Mercouri G. Kanatzidis — Department of Chemistry, Northwestern University, Evanston, Illinois 60208, United States; orcid.org/0000-0003-2037-4168; Email: mkanatzidis@northwestern.edu

Authors

Craig C. Laing — Department of Chemistry, Northwestern University, Evanston, Illinois 60208, United States; orcid.org/0000-0002-0654-4741

Jiahong Shen — Department of Materials Science and Engineering, Northwestern University, Evanston, Illinois 60208, United States

Daniel G. Chica — Department of Chemistry, Northwestern University, Evanston, Illinois 60208, United States;
occid.org/0000-0001-8616-9365

Shelby A. Cuthriell – Department of Chemistry, Northwestern University, Evanston, Illinois 60208, United States

Richard D. Schaller – Department of Chemistry, Northwestern University, Evanston, Illinois 60208, United States; Center for Nanoscale Materials, Argonne National Laboratory, Lemont, Illinois 60439, United States; orcid.org/0000-0001-9696-8830

Chris Wolverton – Department of Materials Science and Engineering, Northwestern University, Evanston, Illinois 60208, United States; orcid.org/0000-0003-2248-474X

Complete contact information is available at: https://pubs.acs.org/10.1021/acs.chemmater.1c01696

Notes

The authors declare no competing financial interest.

ACKNOWLEDGMENTS

This work was supported by the National Science Foundation through the MRSEC program (NSF-DMR-1720139) at the Materials Research Center (C.C.L.) and DMR-2003476 (D.G.C.). This work made use of the Ag-microsource diffractometer in the IMSERC X-RAY facility at Northwestern University to obtain results included in this publication, the purchase of which was supported by the Major Research Instrumentation Program from the National Science Foundation under award CHE-1920248. This work made use of the IMSERC PCM facility at Northwestern University, which has received support from the Soft and Hybrid Nanotechnology Experimental (SHyNE) Resource (NSF ECCS-2025633) and Northwestern University. This work made use of the EPIC facility of Northwestern University's NUANCE Center, which has received support from the SHyNE Resource (NSF ECCS-2025633), the IIN, and Northwestern's MRSEC program (NSF-DMR-1720139). Use of the Center for Nanoscale Materials, an Office of Science user facility, was supported by the U.S. Department of Energy, Office of Science, Office of Basic Energy Sciences, under Contract No. DE-AC02-06CH11357. The authors would like to acknowledge Michael Quintero and Rebecca McClain for productive conversations.

REFERENCES

- (1) Opalovskii, A. A.; Fedorov, V. E.; Lobkov, E. U. The Reaction of Molybdenum, Tungsten and Rhenium Selenides with Gaseous Bromine. *Russ. J. Inorg. Chem.* **1971**, *16*, 790.
- (2) Opalovskii, A. A.; Fedorov, V. E.; Lobkov, E. U.; Erenburg, B. G. New Rhenium Chalcogenide Halides. *Russ. J. Inorg. Chem.* **1971**, *16*, 1685.
- (3) Leduc, L.; Perrin, A.; Sergent, M. Chalcohalides and Chalcogenides with Octahedral Clusters in Low Valency Rhenium Chemistry. C. R. Acad. Sci., Ser. II 1983, 296, 961–966.
- (4) Batail, P.; Ouahab, L.; Pe'nicaud, A.; Lenoir, C.; Perrin, A. Preparation of the tetrabutylammonium salt of a rhenium (III) chalcohalide molecular cluster, $(C_4H_9)_4NRe_6Se_5Cl_9$. C. R. Acad. Sci., Sér. II 1987, 304, 1111–1116.
- (5) Long, J. R.; Williamson, A. S.; Holm, R. H. Dimensional Reduction of $Re_6Se_8Cl_2$: Sheets, Chains, and Discrete Clusters Composed of Chloride-Terminated $[Re_6Q_8]^{2+}$ (Q = S, Se) Cores. *Angew. Chem., Int. Ed.* **1995**, 34, 226–229.
- (6) Long, J. R.; McCarty, L. S.; Holm, R. H. A Solid-State Route to Molecular Clusters: Access to the Solution Chemistry of $[Re_6Q_8]^{2+}$ (Q = S, Se) Core-Containing Clusters via Dimensional Reduction. *J. Am. Chem. Soc.* **1996**, *118*, 4603–4616.
- (7) Willer, M. W.; Long, J. R.; McLauchlan, C. C.; Holm, R. H. Ligand Substitution Reactions of $[Re_6S_8Br_6]^4$: A Basis Set of Re_6S_8 Clusters for Building Multicluster Assemblies. *Inorg. Chem.* **1998**, 37, 328–333.
- (8) Zheng, Z.; Long, J. R.; Holm, R. H. A Basis Set of Re₆Se₈ Cluster Building Blocks and Demonstration of Their Linking Capability: Directed Synthesis of an Re₁₂Se₁₆ Dicluster. *J. Am. Chem. Soc.* **1997**, 119, 2163–2171.
- (9) Wang, R.; Zheng, Z. Dendrimers supported by the $[Re_6Se_8]^{2+}$ metal cluster core. J. Am. Chem. Soc. 1999, 121, 3549–3550.
- (10) Roland, B. K.; Carter, C.; Zheng, Z. Routes to Metallodendrimers of the $[Re_6(\mu_3.Se)_8]^{2+}$ Core-Containing Clusters. *J. Am. Chem. Soc.* **2002**, 124, 6234–6235.
- (11) Roland, B. K.; Selby, H. D.; Cole, J. R.; Zheng, Z. Hydrogen-bonded supramolecular arrays of the $[Re_6(\mu_3-Se)_8]^{2+}$ core-containing clusters. *Dalton Trans.* **2003**, 4307–4312.
- (12) Selby, H. D.; Roland, B. K.; Zheng, Z. Ligand-Bridged Oligomeric and Supramolecular Arrays of the Hexanuclear Rhenium Selenide Clusters—Exploratory Synthesis, Structural Characterization, and Property Investigation. *Acc. Chem. Res.* **2003**, *36*, 933—944.
- (13) Artemkina, S. B.; Naumov, N. G.; Mironov, Y. V.; Sheldrick, W. S.; Virovets, A. V.; Fenske, D. Electroneutral coordination frameworks based on octahedral $[Re_6(\mu_3\text{-}Q)_8(CN)_6]^{4-}$ complexes (Q = S, Se, Te) and the Mn²⁺ cations. *Russ. J. Coord. Chem.* **2007**, 33, 867–875.
- (14) Beauvais, L. G.; Shores, M. P.; Long, J. R. Cyano-Bridged Re₆Q₈ (Q = S, Se) Cluster-Cobalt(II) Framework Materials: Versatile Solid Chemical Sensors. *J. Am. Chem. Soc.* **2000**, *122*, 2763–2772.
- (15) Beauvais, L. G.; Shores, M. P.; Long, J. R. Cyano-Bridged Re_6Q_8 (Q = S, Se) Cluster-Metal Framework Solids: A New Class of Porous Materials. *Chem. Mater.* **1998**, *10*, 3783–3786.
- (16) Kim, Y.; Park, S.-M.; Kim, S.-J. Three-dimensional framework containing Mn(salen)+ and $Re_6Se_8(CN)_6^{4-}$ cluster. *Inorg. Chem. Commun.* **2002**, *5*, 592–595.
- (17) Naumov, N. G.; Artemkina, S. B.; Virovets, A. V.; Fedorov, V. E. Adjustment of dimensionality in covalent frameworks formed by Co^{2+} and rhenium cluster chalcocyanide $\left[Re_6S_8(CN)_6\right]^{4-}$. *Solid State Sci.* **1999**, *1*, 473–481.
- (18) Shestopalov, M. A.; Cordier, S.; Hernandez, O.; Molard, Y.; Perrin, C.; Perrin, A.; Fedorov, V. E.; Mironov, Y. V. Self-Assembly of Ambivalent Organic/Inorganic Building Blocks Containing Re₆ Metal Atom Cluster: Formation of a Luminescent Honeycomb, Hollow, Tubular Metal-Organic Framework. *Inorg. Chem.* **2009**, 48, 1482–1489.
- (19) Yuan, M.; Dirmyer, M.; Badding, J.; Sen, A.; Dahlberg, M.; Schiffer, P. Controlled Assembly of Zero-, One-, Two-, and Three-Dimensional Metal Chalcogenide Structures. *Inorg. Chem.* **2007**, *46*, 7238–7240.

- (20) Gray, T. G.; Rudzinski, C. M.; Nocera, D. G.; Holm, R. H. Highly Emissive Hexanuclear Rhenium(III) Clusters Containing the Cubic Cores $[{\rm Re}_6{\rm S}_8]^{2+}$ and $[{\rm Re}_6{\rm Se}_8]^{2+}$. *Inorg. Chem.* **1999**, 38, 5932–5933.
- (21) Gray, T. G.; Rudzinski, C. M.; Meyer, E. E.; Holm, R. H.; Nocera, D. G. Spectroscopic and Photophysical Properties of Hexanuclear Rhenium(III) Chalcogenide Clusters. *J. Am. Chem. Soc.* **2003**, 125, 4755–4770.
- (22) Kitamura, N.; Ueda, Y.; Ishizaka, S.; Yamada, K.; Aniya, M.; Sasaki, Y. Temperature Dependent Emission of Hexarhenium(III) Clusters $[Re_6(\mu_3-S)_8X_6]^4$ (X = Cl-, Br-, and I-): Analysis by Four Excited Triplet-State Sublevels. *Inorg. Chem.* **2005**, *44*, 6308–6313.
- (23) Guilbaud, C.; Deluzet, A.; Domercq, B.; Molinié, P.; Boubekeur, K.; Batail, P.; Coulon, C. (NBun⁴⁺)3[Re₆S₈Cl₆]³⁻·: synthesis and luminescence of the paramagnetic, open shell member of a hexanuclear chalcohalide cluster redox system. *Chem. Commun.* 1999, 1867–1868.
- (24) Deluzet, A.; Duclusaud, H.; Sautet, P.; Borshch, S. A. Electronic Structure of Diamagnetic and Paramagnetic Hexanuclear Chalcohalide Clusters of Rhenium. *Inorg. Chem.* **2002**, *41*, 2537–2542.
- (25) Kubeil, M.; Stephan, H.; Pietzsch, H.-J.; Geipel, G.; Appelhans, D.; Voit, B.; Hoffmann, J.; Brutschy, B.; Mironov, Y. V.; Brylev, K. A.; Fedorov, V. E. Sugar-Decorated Dendritic Nanocarriers: Encapsulation and Release of the Octahedral Rhenium Cluster Complex [Re₆S₈(OH)₆]⁴⁻. Chem. Asian J. 2010, 5, 2507–2514.
- (26) Echeverría, C.; Becerra, A.; Nuñez-Villena, F.; Muñoz-Castro, A.; Stehberg, J.; Zheng, Z.; Arratia-Perez, R.; Simon, F.; Ramírez-Tagle, R. The paramagnetic and luminescent [Re₆Se₈I₆]³⁻ cluster. Its potential use as an antitumoral and biomarker agent. *New J. Chem.* **2012**, *36*, 927–932.
- (27) Ivanov, A. A.; Konovalov, D. I.; Pozmogova, T. N.; Solovieva, A. O.; Melnikov, A. R.; Brylev, K. A.; Kuratieva, N. V.; Yanshole, V. V.; Kirakci, K.; Lang, K.; Cheltygmasheva, S. N.; Kitamura, N.; Shestopalova, L. V.; Mironov, Y. V.; Shestopalov, M. A. Water-soluble Re₆-clusters with aromatic phosphine ligands from synthesis to potential biomedical applications. *Inorg. Chem. Front.* **2019**, *6*, 882—892.
- (28) Krasilnikova, A. A.; Solovieva, A. O.; Ivanov, A. A.; Trifonova, K. E.; Pozmogova, T. N.; Tsygankova, A. R.; Smolentsev, A. I.; Kretov, E. I.; Sergeevichev, D. S.; Shestopalov, M. A.; Mironov, Y. V.; Shestopalov, A. M.; Poveshchenko, A. F.; Shestopalova, L. V. Comprehensive study of hexarhenium cluster complex $Na_4[\{Re_6Te_8\}-(CN)_6]$ In terms of a new promising luminescent and X-ray contrast agent. Nanomed.: Nanotechnol., Biol. Med. 2017, 13, 755—763.
- (29) Pozmogova, T. N.; Krasil'nikova, A. A.; Ivanov, A. A.; Shestopalov, M. A.; Gyrylova, S. N.; Shestopalova, L. V.; Shestopaloiv, A. M.; Shkurupy, V. A. Studying the Effect of a Composition of the Cluster Core in High-Radiopacity Cluster Complexes of Rhenium on Their Acute Toxicity In Vivo. *Bull. Exp. Biol. Med.* **2016**, *161*, *64*–*68*.
- (30) Kim, Y.; Fedorov, V. E.; Kim, S.-J. Novel compounds based on $[Re_6Q_8(L)_6]^{4-}$ (Q = S, Se, Te; L = CN, OH) and their applications. *J. Mater. Chem.* **2009**, *19*, 7178–7190.
- (31) Kamiguchi, S.; Sayoko, N.; Teiji, C. Catalytic Hydrogenation and Dehydrogenation over Solid-state Rhenium Sulfide Clusters with an Octahedral Metal Framework. *Chem. Lett.* **2007**, *36*, 1340–1341.
- (32) Bruck, A. M.; Yin, J.; Tong, X.; Takeuchi, E. S.; Takeuchi, K. J.; Szczepura, L. F.; Marschilok, A. C. Reversible Electrochemical Lithium-Ion Insertion into the Rhenium Cluster Chalcogenide—Halide Re₆Se₈Cl₂. *Inorg. Chem.* **2018**, *57*, 4812–4815.
- (33) Choi, B.; Lee, K.; Voevodin, A.; Wang, J.; Steigerwald, M. L.; Batail, P.; Zhu, X.; Roy, X. Two-Dimensional Hierarchical Semi-conductor with Addressable Surfaces. *J. Am. Chem. Soc.* **2018**, *140*, 9369–9373.
- (34) Zhong, X.; Lee, K.; Choi, B.; Meggiolaro, D.; Liu, F.; Nuckolls, C.; Pasupathy, A.; De Angelis, F.; Batail, P.; Roy, X.; Zhu, X. Superatomic Two-Dimensional Semiconductor. *Nano Lett.* **2018**, *18*, 1483–1488.

- (35) Gabriel, J.-C. P.; Boubekeur, K.; Uriel, S.; Batail, P. Chemistry of Hexanuclear Rhenium Chalcohalide Clusters. *Chem. Rev.* **2001**, 101, 2037–2066.
- (36) Fischer, C.; Alonso-Vante, N.; Fiechter, S.; Tributsch, H.; Reck, G.; Schulz, W. Structure and photoelectrochemical properties of semiconducting rhenium cluster chalcogenides: $Re_6X_8Br_2$ (X = S, Se). *J. Alloys Compd.* **1992**, *178*, 305–314.
- (37) Fischer, C.; Fiechter, S.; Tributsch, H.; Reck, G.; Schultz, B. Crystal Structure and Thermodynamic Analysis of the New Semiconducting Chevrel Phase Re₆S₈Cl₂. *Ber. Bunsenges. Phys. Chem.* **1992**, *96*, 1652–1658.
- (38) Pilet, G.; Hernandez, O.; Perrin, A. Crystal structure of rhenium caesium sulfobromide, CsRe₆S₈Br₃, the first cluster compound in the Cs-Re-S-Br system exhibiting two types of interunit bridges. *Z. Kristallogr. New Crystal Struct.* **2002**, 217, 11–12.
- (39) Pilet, G.; Perrin, A. New compounds in the cesium sulfobromide rhenium octahedral cluster chemistry: syntheses and crystal structures of Cs₄Re₆S₈Br₆ and Cs₂Re₆S₈Br₄. *Solid State Sci.* **2004**. *6*. 109–116.
- (40) Perrin, A.; Leduc, L.; Potel, M.; Sergent, M. New quaternary rhenium chalcohalides with octahedral Re₆ clusters: $MRe_6Y_5X_9$ M = univalent cation, X = halogen, Y = chalcogen. *Mater. Res. Bull.* **1990**, 25, 1227–1234.
- (41) Perricone, A.; Slougui, A.; Perrin, A. Rhenium octahedral clusters: the systems Re-S-Br and M-Re-S-Br (M = Na, K, RB, Cs). *Solid State Sci.* **1999**, *1*, 657–666.
- (42) Yarovoi, S. S.; Mironov, Y. V.; Tkachev, S. V.; Fedorov, V. E. Phase formation in the Re-Se-Br-MBr systems (M = Li, Na, K, Rb, Cs). Russ. J. Inorg. Chem. 2009, 54, 299–304.
- (43) Speziali, N. L.; Berger, H.; Leicht, G.; Sanjinés, R.; Chapuis, G.; Lévy, F. Single crystal growth, structure and characterization of the octahedral cluster compound Re₆Se₈Br₂. *Mater. Res. Bull.* **1988**, 23, 1597–1604.
- (44) Leduc, L.; Padiou, J.; Perrin, A.; Sergent, M. Synthèse et caractérisation d'un nouveau chalcohalogénure à clusters octaédriques de rhénium à caractère bidimensionnel: Re₆Se₈Cl₂. *J. Less-Common Met.* **1983**, 95, 73–80.
- (45) Leduc, L.; Perrin, A.; Sergent, M. Structure du dichlorure et octaséléniure d'hexarhénium, Re₆Se₈Cl₂: composé bidimensionnel à clusters octaédriques Re₆. *Acta Crystallogr., Sect. C* **1983**, 39, 1503–1506.
- (46) DeVries, T.; Rodebush, W. H. The Thermal Dissociation of Iodine and Bromine. J. Am. Chem. Soc. 1927, 49, 656-666.
- (47) STOE & Cie GmbH. X-area (version 1.90); X-red (version 1.65.2); X-Shape (version 2.21); STOE LANA (version 1.83.8), 2020.
- (48) Sheldrick, G. SHELXT Integrated space-group and crystal-structure determination. *Acta Crystallogr., Sect. A* **2015**, *71*, 3–8.
- (49) Dolomanov, O. V.; Bourhis, L. J.; Gildea, R. J.; Howard, J. A. K.; Puschmann, H. OLEX2: a complete structure solution, refinement and analysis program. *J. Appl. Crystallogr.* **2009**, *42*, 339–341.
- (50) Sheldrick, G. Crystal structure refinement with SHELXL. *Acta Crystallogr., Sect. C* **2015**, *71*, 3–8.
- (51) Hohenberg, P.; Kohn, W. Inhomogeneous Electron Gas. *Phys. Rev.* **1964**, *136*, No. B864.
- (52) Kohn, W.; Sham, L. J. Self-Consistent Equations Including Exchange and Correlation Effects. *Phys. Rev.* **1965**, *140*, No. A1133.
- (53) Kresse, G.; Furthmüller, J. Efficiency of ab-initio total energy calculations for metals and semiconductors using a plane-wave basis set. *Comput. Mater. Sci.* **1996**, *6*, 15–50.
- (54) Kresse, G.; Furthmüller, J. Efficient iterative schemes for ab initio total-energy calculations using a plane-wave basis set. *Phys. Rev. B* **1996**, *54*, No. 11169.
- (55) Blöchl, P. E. Projector augmented-wave method. *Phys. Rev. B* **1994**, 50, No. 17953.
- (56) Perdew, J. P.; Burke, K.; Ernzerhof, M. Generalized Gradient Approximation Made Simple. *Phys. Rev. Lett.* **1996**, *77*, No. 3865.
- (57) Togo, A.; Tanaka, I. First principles phonon calculations in materials science. *Scr. Mater.* **2015**, *108*, 1–5.

- (58) Barber, C. B.; Dobkin, D. P.; Huhdanpaa, H. The quickhull algorithm for convex hulls. *ACM Trans. Math. Software* **1996**, 22, 469–483.
- (59) Saal, J. E.; Kirklin, S.; Aykol, M.; Meredig, B.; Wolverton, C. Materials Design and Discovery with High-Throughput Density Functional Theory: The Open Quantum Materials Database (OQMD). *JOM* **2013**, *65*, 1501–1509.
- (60) Kirklin, S.; Saal, J. E.; Meredig, B.; Thompson, A.; Doak, J. W.; Aykol, M.; Rühl, S.; Wolverton, C. The Open Quantum Materials Database (OQMD): assessing the accuracy of DFT formation energies. npj Comput. Mater. 2015, 1, No. 15010.
- (61) Wasilevski, R. Physical and mechanical properties of rhenium. *Trans. Metall. Soc. AIME* **1961**, 221, 1081–1082.
- (62) Bennett, M. J.; Cotton, F. A.; Foxman, B. M. Crystal and molecular structure of trirhenium nonaiodide. *Inorg. Chem.* **1968**, *7*, 1563–1569.
- (63) Lamfers, H. J.; Meetsma, A.; Wiegers, G. A.; de Boer, J. L. The crystal structure of some rhenium and technetium dichalcogenides. *J. Alloys Compd.* **1996**, *241*, 34–39.
- (64) Yamashita, D.; Ishizaki, A. In situ measurements of change in work function of Pt, Pd and Au surfaces during desorption of oxygen by using photoemission yield spectrometer in air. *Appl. Surf. Sci.* **2016**, 363, 240–244.
- (65) Harwell, J. R.; Baikie, T. K.; Baikie, I. D.; Payne, J. L.; Ni, C.; Irvine, J. T. S.; Turnbull, G. A.; Samuel, I. D. W. Probing the energy levels of perovskite solar cells via Kelvin probe and UV ambient pressure photoemission spectroscopy. *Phys. Chem. Chem. Phys.* **2016**, *18*, 19738–19745.
- (66) Kortüm, G.; Braun, W.; Herzog, G. Prinzip und Meßmethodik der diffusen Reflexionsspektroskopie. *Angew. Chem.* **1963**, *75*, 653–661.
- (67) Perdew, J. P.; Yang, W.; Burke, K.; Yang, Z.; Gross, E. K. U.; Scheffler, M.; Scuseria, G. E.; Henderson, T. M.; Zhang, I. Y.; Ruzsinszky, A.; Peng, H.; Sun, J.; Trushin, E.; Görling, A. Understanding band gaps of solids in generalized Kohn–Sham theory. *Proc. Natl. Acad. Sci. U.S.A.* **2017**, *114*, 2801.